PAPER

Loss of spin polarization in ferromagnet/ferroelectric tunnel junctions due to screening effects

IOP ebooks™

Bringing you innovative digital publishing with leading voices to create your essential collection of books in STEM research.

Start exploring the collection - download the first chapter of every title for free.

Loss of spin polarization in ferromagnet/ferroelectric tunnel junctions due to screening effects

C Sen[1], W A S Aldulaimi[1], O Mohammadmoradi[1] and I B Misirlioglu[1,2,3,4]

[1] Faculty of Engineering and Natural Sciences, Sabancı University, Orhanlı/Tuzla 34956 Istanbul, Turkey
[2] Integrated Manufacturing Technologies Research and Application Center, Sabanci University, Tuzla, 34956 Istanbul, Turkey
[3] Sabancı University Nanotechnology Application Center, Orhanlı/Tuzla 34956 Istanbul, Turkey

E-mail: burc@sabanciuniv.edu

CrossMark

Abstract

Electric field control of magnetization allows further miniaturization of integrated circuits for binary bit processing and data storage as it eliminates the need for bulky sophisticated systems to induce magnetic fields. Magnetoelectric coupling inherent to the bulk of multiferroic films or control of spin orientation in magnetic layers via piezoelectric strain in dual component composites have been two approaches standing out. Another magnetoelectric effect is spin-dependent screening that occurs at dielectric/ferromagnet interfaces which is of great importance for spin selective tunnel junctions. Here, we analyze the spin-dependent screening of ferroelectric polarization in a film interfacing ferromagnetic electrodes using the continuity equations in continuum media. The competition between the electrostatic and the magnetochemical potential in the FM electrodes gives rise to a reduction in the net magnetic moment near the interface due to spin mixing, extending to a distance comparable to the Thomas–Fermi screening length. Our continuum media treatment shows that the local spin population in spin subbands near the interfaces can dramatically deviate from bulk, which is in qualitative agreement with recent first principles results. We compute the tunneling currents for the majority and minority spins using the Wentzel–Kramers–Brillouin approximation as a function of ferroelectric polarization. We find that the spin polarization tends to disappear for increasing values of ferroelectric polarization in direct connection with the increase in subband spin population for minority spins at the interface.

Keywords: ferroelectric films, tunnel magnetoresistance, ferromagnetic electrodes

(Some figures may appear in colour only in the online journal)

1. Introduction

Magnetoelectric coupling in bulk of perovskite oxides has been a forthcoming topic of interest since the observation of this phenomena near or above room temperature in ABO_3 type oxides. A is usually a rare earth and B is a transition metal element hosting spins when in the elemental state with O sites aiding in double-exchange between B sites generating long range magnetic ordering. The manifestation of the Dzyhalozhinski–Moriya coupling in some rare earth based perovskites [1–4] has paved the way to prescribe compositions that would allow coexistence of magnetic and electrical ordering in the bulk of a number of cubic perovskite materials. The symmetry correlation between the spontaneous electrical dipole order and the magnetic dipoles in the unit cell of such materials has allowed manipulating one order parameter via control of the other [5, 6]. From a technological point of view, control of the magnetic order through electric fields has been

[4] Author to whom any correspondence should be addressed.

J. Phys. D: Appl. Phys. **52** (2019) 015305

C Sen *et al*

rather attractive as this would eliminate bulky components required to generate magnetic fields [7–12]. Several magnetoelectric oxides manifest magnetism by mechanisms such as double-exchange between B-sites via oxygen sites and is of ionic origin [2, 13–21] that give rise to a small but finite ferroelectric (FE) polarization, namely 'improper ferroelectricity' [22]. In fact, many material systems investigated in the past decade under the title of multiferroic behavior fall into this category. Dual phase systems where the material is microscopically engineered to exhibit two distinct phases with each phase having its own order parameter have also been on the agenda of research groups in attempts to create extrinsic multiferroicity [23–34]. These systems usually rely on the strain sensitivity of both magnetic and electrical order parameters in the distinct phases. Inducing strain in one component via an electric field that alters spin alignment in the magnetic phase via magnetostriction has been the key parameter to generate the magnetoelectric coupling between the two order parameters in a composite-like dual phase system.

Another type of magnetoelectric coupling that is inherent to dielectric/FM interfaces occurs due to spin dependent screening. Contrary to the numerous efforts focusing on multiferroic compositions and composites, there are a handful of works that focus on this mechanism at dielectric/ferromagnet (DE/FM) interfaces [35–37]. Upon application of a bias to a contact between a DE and a FM conductor, the screening of the polarization charges induced on the dielectric side of the interface becomes spin dependent. This naturally occurs because carriers accumulating or depleting the interface on the FM side are subject to the exchange field, hence the subband density of states (DOS) differ for spins of opposite sign. The DOS for the up and down spins in the valence band of the FM are shifted along the energy axis by an amount proportional to the strength of the internal exchange field whose origins are quantum mechanical. This situation can be altered by the polarization charges from the DE side when under bias and can be quite significant especially in thin film junctions where the screening lengths can become comparable to film thickness. Thus, a relatively high bias applied to a dielectric/FM junction can generate strong changes in the interface magnetization of the FM, either enhancing it or degrading it depending on whether accumulation or depletion of spins occurs due to local electrostatics. It has been reported that a very small change occurs in the interface magnetization of metallic FMs [38] as the screening lengths are very short owing to the very large density of states near the Fermi level, for instance in 3d metals. In FM oxides, on the other hand, that recently attracted great attention, changes amounting to 50% or more in the interface magnetization at distance of about 10 nm or more have been reported [39–41]. The main mechanism of such dramatic changes in interface magnetization of FM oxides can be shown to be purely due to the accumulation/depletion behavior of a doped semiconductor with the only difference that the carriers are spin polarized.

Spin accumulation and depletion at interfaces through the application of a bias via the mechanism mentioned above forms the basis on which magnetoresistive junctions operate, in particular, the junctions where the tunnel magnetoresistive (TMR) effect is tailored [42–51]. In conventional FM/DE/FM TMR stacks, one can obtain spin polarized tunnelling currents that are determined by the spin states of electrons in the FM electrodes. TMR junctions consist of two FMs separated by a thin layer of dielectric, a corollary of the Giant Magnetoresistive (GMR) stack. The spin polarization and magnitude of currents across a TMR stack depends on the relative orientation of the magnetism in the FM electrodes and a bias simply controls the electrical barrier to spin tunneling via the polarization of the dielectric. Shortly after the demonstration of the TMR effect in FM/DE/FM thin film stacks, replacing the DE with a ferroelectric (FE) layer entered the agenda of the scientific groups working on the development of devices for spintronics. The driving force behind such a pursuit was that the FE polarization can dramatically alter the on/off ratios of spin currents depending on the direction of remnant dipoles as they can easily be switched under a few volts of bias. FE TJs sandwiched between metal and semiconductor electrodes have already been proven to generate on/off ratios reaching 10^3–10^5 [52–58].

Inspired by results from to metal/FE/semiconductor junctions, a distinct control of spin currents in a gate-like setting via the FE layer appears to be an attractive option due to the ratio of the on/off states of spin currents that can vary by several orders of magnitude [34, 59–61]. TMR in FE TJs has been studied but similar to the TMR effect in FM/DE/FM stacks with the DE as the TJ, loss of spin polarization in tunnelling currents at moderate to high bias values is a persisting problem [62–64] even in the case of magnetization being parallel in the FM electrodes. The origins of such an outcome has been discussed extensively by a few authors for DE TJs [47, 65–67]. The flipping of the spins of 'hot' electrons (those who have gained energy above the Fermi level of the FM electrodes) following tunnelling, magnon excitations and scattering events from defects inside the TJ that induce spin flips were discussed as major scenarios degrading the TMR effect. The changes in interface states in TJ/FM junctions has been mentioned in a few works [35, 67]. From the continuum media perspective one would expect a competition between electrostatic and magnetochemical potential an electron feels near a dielectric/FM interface under bias, keeping in mind magnetochemical potential pushes minority carriers to higher energies (some of which flip their spins and become majority carriers) via band shifts and charge distribution occurs always to minimize electrostatic energy. The finite penetration of the electric field to the surface of a metallic FM in a dielectric/FM junction under a potential drop will mostly be screened by majority spin electrons of the FM near the Fermi level. Strong electric fields could require carrier densities much greater than the population density allowed by the subband DOS of the majority spins. It can thus be expected that minority spin carriers can take effect and participate in the screening process as long as the energy difference between the spin subbands is not extreme such as in the case of half-metals. FEs can generate very strong fields near a metallic or semiconductor interface and pave a way to effectively manipulate carriers as well as their spins.
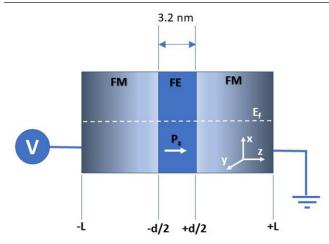
J. Phys. D: Appl. Phys. **52** (2019) 015305

C Sen *et al*

Figure 1. The schematic of the FM/FE/FM stack used to compute the spin dependent screening process in this work. Bias is applied to the left FM electrode, E_F denotes the Fermi level. Right electrode is grounded.

Here, we aim to understand the effect of the electrostatic screening process of FE polarization charges on magnetoresistive effects. For this purpose, we study a FM/FE/FM stack using the continuity equations in continuum media and study the spin dependent screening at the FM interfaces that has important implications for obtaining the TMR effect from such structures. The competition between the electrostatic and the magnetochemical potential of carriers at the FE/FM interfaces is demonstrated. Spin mixing, namely reduction of the majority/minority spin population ratio, could occur at the interfaces where the local density of states (LDOS) for minority spins is greater than in that of the bulk. This is driven by the need to screen polarization charges if the FE layer has a relatively strong polarization or is under a strong bias. By considering majority and minority spin channels, we try to quantify the limits of FE polarization and applied bias beyond which spin polarized currents are unlikely that would result in reduction of the TMR. We prove so by directly computing the tunnelling currents for majority and minority spin channels using the Wentzel–Brillouin–Kramers (WKB) approximation and discuss the results in the light of barrier heights for the two spin channels.

2. Theoretical approach

2.1. Spin dependent electrostatics

We consider an ultrathin FE layer sandwiched between two FM electrodes as shown schematically in figure 1. The FM electrodes are assumed to be sufficiently thick that away from the FE interface the bulk properties are recovered. The FE layer sees the bias via assigning a desired electrical potential to the left FM electrode between $-L$ and $-d/2$ (see figure 1). For demonstrative purposes, one can also analyze a DE layer sandwiched between FM electrodes where one only has to drop the P_z term from the equations and assign a linear dielectric displacement to the TJ. We fixed the FE thickness to 3.2 nm as this fall into an approximate median of many experimental works [59, 68–70]. For the case of FE

in thermodynamic equilibrium, we assign a small compressive misfit to the FE layer structure allowing us to treat the FE regime with the polarization pointing along the normal of the TJ layer. We mention this point here as we compute the spin population near the Fermi level for non-equilibrium (or 'imposed') polarization and polarization obtained from thermodynamic theory. In a ferroelectric sandwiched between FM electrodes, the Maxwell equation

$$\nabla \cdot D = \rho \qquad (1)$$

has to be satisfied at every point under any given boundary condition. Here ρ is the charge density and D is the dielectric displacement vector. Equation (1) holds inside the FM and for an ideal, insulating FE, $\rho = 0$ and thus $\nabla \cdot D = 0$ in the latter. Due to the symmetry of the stack along the plane, we reduce the problem into 2 dimensions as shown in figure 1. We can thus write D as

$$D = D_x\widehat{x} + D_z\widehat{z} \qquad (2)$$

where

$$D_x = \varepsilon_0\varepsilon_b E_x + P_x \text{ and } D_z = \varepsilon_0\varepsilon_b E_z + P_z \qquad (3)$$

in the FE layer with x and z denoting the in-plane and out-of-plane components respectively and,

$$D_x = \varepsilon_0\varepsilon_r E_x \text{ and } D_z = \varepsilon_0\varepsilon_r E_z \qquad (4)$$

in the FM electrodes having a lattice dielectric constant of ε_r taken as 10. In equations (3) and (4), ε_0 is the permittivity of the vacuum and ε_b is the background dielectric constant of the FE (10 in this work [71, 72]), E_x and E_z are respectively the x- and z- components of the electric field vector E that can be determined from $E_x = -\partial\phi/\partial x$ and $E_z = -\partial\phi/\partial z$ with ϕ being the electrostatic scalar potential, P_x and P_z are the FE polarization components along x- and z-axes respectively. ρ is the spatial total charge density and consists of electrons and ionized ions that donate these electrons in the electrode:

$$\rho = q(-n^- + N_D^+). \qquad (5)$$

The effect of ferromagnetism can be accounted for in the calculations of the charge distribution. We treat the FM electrode as a medium with positively ionized donors and a large density of states near the Fermi level (10^{27} m^{-3}, similar to that of DFT results yielded for Fe, [73]) with electron population that fill these available states (see figure 2 for the schematic). The latter is a common phenomenon in 3d transition metals and 4f lanthanides exhibiting magnetic ordering where the net spin can be maximized in accordance with the Hund's rule as the very large DOS in the 3d and 4f bands permit this. In the bulk of the FM, the electric field is zero and thus $\rho = 0$. Here, the carrier distribution as well as the DOS in the bands involve the presence of the magnetic exchange giving rise to FM state that can be accounted for in a fashion similar to the Pauli paramagnetism. We follow a route identical to the approximation outlined in [74] where the DOS in a band can be thought of as 2 subbands, namely DOS for up-spins and DOS for down-spins. The mean exchange field aligns the spins where one sign of spin is favored over the other thus generating a net non-zero magnetic dipole moment density inside the electrode.
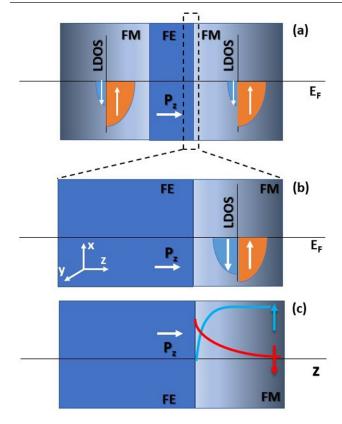
Figure 2. The schematic for (a) the spin subband DOS, (b) shift of spin subband DOS near the interface with respect to the bulk and (c) resulting in spatial spin distribution near the interface.

From here onwards we will call up-spins 'majority spins' and down-spins 'minority spins'. The pseudospins in the real lattice pointing in any crystallographic direction consists of mathe jority and minority spins that form the basis states, thus the difference between the majority spin and minority spin concentrations caused by the mean exchange field is the origin of FM behavior. Note that we are not concerned with the crystallographic direction of magnetism as this consideration is related to what one calls 'pseudo spin' orientation that can be expressed in terms of the majority spin and minority spin basis states via the Pauli matrices. To account for screening effects, one needs to know the majority spin and minority spin band DOS and the corresponding population density (determined by the Fermi–Dirac distribution) only. In this context, the number of available states per unit volume for each spin subband $g(E)$ near the Fermi level (E_F) can be approximated as

$$g(E)_\uparrow = \frac{1}{2} \int_{E_F}^{E_F + kT} (N_c + g(H_m \mu_b)) \, dE \qquad (6)$$

for the up-spins (majority spins) and

$$g(E)_\uparrow = \frac{1}{2} \int_{E_F}^{E_F + kT} (N_c - g(H_m \mu_b)) \, dE \qquad (7)$$

for the down (minority) spins. Here, N_c is the DOS at the Fermi level in the paramagnetic state, H_m is the mean exchange field inside the magnetic medium, μ_b is the Bohr magneton, $g(H_m \mu_b)$ represent the DOS corresponding to an energy $H_m \mu_b$ near Fermi level. The $g(H_m \mu_b)$ term is added to the

Table 1. The material constants and band parameters used in the numerical calculations.

	$g(E_F)$ (m^{-3}),	E_f, E_c, E_v (eV)	H_0 (T)	N_D (m^{-3})
FM	$10^{27}, 10^{27a}$	-4.5	500	10^{27}
FE	Not considered (insulator limit)	$-5.0, -3.2, -5.5$	—	—

^{a} Divide by 2 for the majority and minority subband DOS in the paramagnetic state.

majority spin DOS and is subtracted from the minority spin DOS as there is a transfer of available states corresponding to an energy of $H_m \mu_b$ for a positive H_m, i.e. the magnetochemical potential determines the shift of subbands of spins. In a FM metal such as Fe, this shift can be quite strong due to the strength of the internal exchange field (at the order of 500 T). We here approximate this shift to be occurring only near the Fermi level as $g(H_m \mu_b) \ll E\_DOS\_total$ where DOS_total is the energy range of the total density of states in the relevant band. The mean exchange field, H_m, is of quantum mechanical origin and is assumed constant inside the bulk of the FM medium where $E = 0$. Considering the dependence of the FM order on carriers, namely the itinerant contribution, H_m is naturally sensitive to carrier, hence, spin density and can be modified approximately for charge redistribution in case of electric field penetration into the magnetic medium as

$$H_m = H_0 + w \mu_b \left(n_\uparrow^+ - n_\downarrow^+ \right) \qquad (8)$$

for a material such as Fe or Co, H_0 is the mean exchange field in the bulk of the FM, w is a coupling coefficient (taken as unity here, see [74]). The approach laid above is sometimes known as the Stoner–Wohlfarth model to introduce the spin dependence of DOS, i.e. the subband available states. In the FM electrode, the Fermi level lies inside the conduction band. The majority spins aligned parallel to H_m will have a larger share of the band states than those that are antiparallel to H_m. One can thus write n^- (namely the population density) and N_D^+ terms in equations (5) and (8) as

$$N_D^+ = N_D \left[\left(\exp\left(\frac{q(E_D - E_F - \phi)}{kT} \right) + 1 \right)^{-1} \right] \qquad (9)$$

$$n_\uparrow^- = g(E)_\uparrow \left(\exp\left(\frac{q(E_C - E_F - \phi) - \mu_b H_m}{kT} \right) + 1 \right)^{-1} \qquad (10)$$

$$n_\downarrow^- = g(E)_\downarrow \left(\exp\left(\frac{q(E_C - E_F - \phi) + \mu_b H_m}{kT} \right) + 1 \right)^{-1} \qquad (11)$$

at a given coordinate inside the FM electrode. In equations (9)–(11) N_D^+ (N_D) is the ionized (total) donor density in the FM electrode of the FE film. n^- is the electron density written for the majority spin and minority spin subbands, $g(E)$ have their usual meanings as denoted in equations (6) and (7). E is the energy of an electron at the top of the valence band at a given coordinate in the FM electrode, E_F is the Fermi level, ϕ is the local electrostatic potential, $\mu_b H_m$ is the magnetochemical potential a carrier feels depending on its spin. The sign of this

J. Phys. D: Appl. Phys. **52** (2019) 015305

C Sen *et al*

term is $-$ for majority spins and $+$ for minority spins. All the band parameters for FM and the FE are given in table 1. The Fermi level of the stack is assumed to be equal to that of the FM electrode, which we take as that of Fe here. Electrostatic (for the potential) and non-electrostatic boundary conditions (for the polarization) are needed to obtain solutions to the above equations. The boundary conditions for the electrostatic potential is:

$$\varnothing_{FE} = \varnothing_{FM}\big|_{z=-\frac{d}{2},\frac{d}{2}} \text{ and } \frac{d\varnothing}{dz} = 0\bigg|_{-L,+L} \quad (12)$$

implying the continuity of the potential at the FE/FM interfaces, where $\varnothing_{FE}$ and $\varnothing_{FM}$ are the electrostatic potentials inside the FE and the FM electrodes respectively and second differential BC in equation (12) indicates the absence of electric field away from the FE/FM interfaces. Polarization BCs are given in the section 2.3. The bias forming the electric field on the system is always assigned to the LHS FM electrode while the RHS electrode is kept grounded, similar to experiments. Periodic boundary conditions (BCs) are employed along the plane of the structures for both the electrostatic potential and polarization. One can approximate the volumetric magnetic dipole moment density obtained from:

$$M = \mu_b\left(n_\uparrow^- - n_\downarrow^-\right) + \mu_b N_d^+ \quad (13)$$

where the first term on the RHS is the itinerant contribution and the second term is the contribution from ionic sites in the lattice. One would thus expect a competition between electrostatic screening and M through the charge distribution function noting that $H_m = \mu_b H_0 + w\mu_b\left(n_\uparrow^- - n_\downarrow^-\right)$. Throughout the work, the value of H_m has the same sign in the LHS and RHS FM electrodes corresponding to parallel magnetization as this allows us to identify FE polarization effects distinctly. Different signs of H_m would mean different relative orientation of the magnetization in the layers corresponding to different subband DOS in the FM electrodes. The effect of relative magnetic orientations on magnetoresistance is well-understood since the first papers of Fert group and Grünberg group [75–77] and is not considered here. We shall, however, show in Results and Discussion that FE polarization impacts locally the subband DOS hence the spin population at the interfaces for positive H_m on LHS and RHS FM electrodes, changing the local magnetization amplitude of FM electrodes.

2.2. Homogeneous polarization approximation

In the course of the work, we noticed that there are additional complications that arise from possible inhomogeneities in the ferroelectric polarization of the tunnel junction. To be able to provide an overall view of the connection between the magnetoelectric coupling occurring due to spin dependent screening and polarization strength, we first assume a linear connection between the electric field and a uniaxial polarization inside the ferroelectric layer via

$$D_z = \epsilon_o \epsilon_b E_z + P_z \text{ and } div D_z = 0 \quad (14)$$

where we assign P_z in the FE layer any value between -0.3 and 0.3 C m^{-2} that are well within the range of the zero field calculated values for homogeneously strained thin FE films between electrodes. The space charge density in the FE layer is assumed to be zero (see equation (14)) for convenience as considering the wide bandgap nature of the FE (such as BaTiO$_3$ (BT)) does not produce any meaningful differences in the barrier height. Note that the above mentioned polarization values might or might not correspond to equilibrium (hence we call is 'imposed' or 'non-equilibrium' polarization) and a homogeneous profile of P_z across the film thickness is supposed. Despite this, the relevant depolarizing field effects and their connection with the spin dependent screening under any bias value can be calculated: one only needs to solve the electric field, E_z, everywhere inside the FM electrodes and FE. The 'fixed P_z' assumption is valid for the bias duration being much less than polarization relaxation of the FE. Inside the FM electrodes, equations (1) and (5) hold. To demonstrate a TJ with a linear dielectric, one only needs to drop the P_z term in equation (14) and replace ϵ_b with ϵ_r, namely the relative dielectric constant of the dielectric. We skip the case of a DE TJ as this is well understood since 1990s where a relatively weak dependence on the dielectric constant of the TJ is expected. On the other hand, the reported bias dependence of the TMR behavior of dielectric TJs are somewhat parallel with that of a FE TJ as we shall show here with the difference that the latter has much greater on/off current ratios.

2.3. Polarization obtained from thermodynamic equation of state

While the electric field is connected to the dielectric properties of the FM electrodes and FE via equations (1) (for $\rho = 0$) and (3), Landau–Ginzburg equations of state for polarization also have to be solved in the FE layer:

$$2\alpha_3^m P_z + 4\alpha_{13}^m P_z P_x^2 + 4\alpha_{33}^m P_z^3 + 6\alpha_{111} P_z^5$$
$$+\alpha_{112}\left(4P_z P_x^4 + 8P_z^3 P_x^2\right) + 2\alpha_{123} P_z P_x^4 - G\left(\frac{\partial^2 P_z}{\partial z^2} + \frac{\partial^2 P_z}{\partial x^2}\right) = -\frac{\partial \phi}{\partial z}$$
$$(15)$$

$$2\alpha_1^m P_x + 2\left(2\alpha_{11}^m + \alpha_{12}^m\right)P_x^3 + 2\alpha_{13}^m P_x P_z^2 + 6\alpha_{111} P_x^5$$
$$+2\alpha_{112}\left[3P_x^5 + 3P_x^3 P_z^2 + P_x P_z^4\right] + 2\alpha_{123} P_x^3 P_z^2 - G\left(\frac{\partial^2 P_x}{\partial z^2} + \frac{\partial^2 P_x}{\partial x^2}\right) = -\frac{\partial \phi}{\partial x}$$
$$(16)$$

and simultaneously satisfy equation (1) when $\rho = 0$. To avoid any *a priori* assumptions on the direction of FE polarization, we considered an in-plane component of polarization, P_x in addition to the out-of-plane component due to size effects and the possibility of domain formation in the TJ. We, however, find a single domain uniaxial state that has been demonstrated in experiments focusing on tunnelling resistance. Note that thermodynamic stabilization of a single domain state in ultrathin FE layers can be expected due to the energy cost of the domain wall formation in such structures that was even reported in ferroelectric/paraelectric superlattices [78–80]. Hence, for sufficient compressive strains ($> -1\%$ or more here), one can safely eliminate the component P_x in equations (15) and (16) and solve it only for P_z in the limit

of uniaxial FE polarization. In equations (15) and (16) α_3^m, α_{13}^m, α_{33}^m, α_1^m, α_{11}^m, α_{12}^m are the renormalized phenomenological thermodynamic coefficients [71] in SI units with α_1^m and α_3^m being $\alpha_1^m = \alpha(T - T_c) - 2u_{ij}^M(Q_{11} + Q_{12})/(S_{11} + S_{12})$ and $\alpha_3^m = \alpha(T - T_c) - 2u_{ij}^M Q_{12}/(S_{11} + S_{12})$ due to renormalization with misfit strain where $\alpha = (2\varepsilon_o C)^{-1}$, α_{12}^m and α_{33}^m contain the clamping effect of the film, while α_{111}, α_{112}, α_{123} are the dielectric stiffness coefficients in the bulk, u_{ij}^M is the misfit strain tensor for a cubic structure and its diagonal, non-zero in-plane components are taken here either as -1.25% or -1.5% (negative here meaning compression) that keeps the FE polarization along the normal of the stack plane. The two different misfit values produce different polarization amplitudes allowing us to study the effect of this parameter on spin polarization of the tunneling currents. In equations (15) and (16), G is the gradient energy coefficient and is assumed to be isotropic for convenience. All the phenomenological coefficients used in the thermodynamic calculations are for BT and are compiled from [81]. The polarization boundary conditions at the LHS and RHS interfaces are important as previously discussed [82, 83] and can be expressed as

$$\left[P_z + \lambda\frac{dP_z}{dz}\right]_{z=-d/2,+d/2} = 0, \quad \left[P_x + \lambda\frac{dP_x}{dz}\right]_{z=-d/2,+d/2} = 0 \tag{17}$$

with z indicating the coordinates for left FM/FE and right FE/FM interfaces, λ is the extrapolation length determining the extent of the change of polarization along the film normal at the interface and is a parameter implying how polarization terminates at the interfaces (taken as 3 nm here based on previous reports [84]). We employ a finite difference discretization in 2D and carry out a Gauss–Seidel iterative scheme to solve the coupled equations (1), (5), (9)–(11), (15) and (16) simultaneously subject to the relevant BCs provided above in the case of homogeneous and equilibrium polarization states whose results we discuss in the next sections. The computation grid consists of 200×400 points where h is the distance between the nearest nodes both along x- and z-axes with a value equal to the unit cell of BCC Fe (~2 angstroms), where n is the number of nodes whose sum gives the FM/FE/FM trilayer thickness (40 nm total). We terminate the solution after 10 000 iterations that yield a difference of less than 10^{-4} for $\varnothing$ and P between two consecutive steps. All results here are provided for room temperature calculations.

2.4. Calculation of the spin polarized tunnel currents

The tunneling currents for the majority spins and minority spins across the FE TJ can be calculated using the dual spin channel approximation where the current for a given sign of spin depends on the population density of that spin at the interface as well as the barrier modified by the magnetochemical potential for that spin and the relative ratio of the subband available states in the opposite electrodes. The total current J is then

$$J = J_\uparrow + J_\downarrow \tag{18}$$

where

$$J_\uparrow = N_\uparrow T_\uparrow(E)\,v \text{ and } J_\downarrow = N_\downarrow T_\downarrow(E)\,v. \tag{19}$$

In equation (19) above, $N_\uparrow$ and $N_\downarrow$ are the population densities of majority and minority spins at the FE/FM interface on the FM side (RHS electrode in figure 1 taken as the reference), $T_\uparrow(E)$ and $T_\downarrow(E)$ are the transmission probabilities of the up- and minority spins and v is the Richardson velocity found from $v = \sqrt{2kT/m^*}$ where m^* is the effective mass of the electrons near the bottom of the conduction band of BT. $T_\uparrow(E)$ and $T_\downarrow(E)$ are obtained from the WKB approach for an arbitrary potential barrier at any coordinate r, $V(r)$ inside of the turning points of the electrostatic potential given by

$$T_\uparrow(E) = \frac{g(E)_\uparrow}{g(E)_\uparrow + g(E)_\downarrow}A\prod_{-d/2}^{d/2}\exp\left(\frac{\Delta d}{\hbar}\sqrt{2m^*(V_\uparrow(r) - E(V_{app}))}\right) \tag{20}$$

$$T_\downarrow(E) = \frac{g(E)_\downarrow}{g(E)_\uparrow + g(E)_\downarrow}A\prod_{-d/2}^{d/2}\exp\left(\frac{\Delta d}{\hbar}\sqrt{2m^*(V_\downarrow(r) - E(V_{app}))}\right) \tag{21}$$

with the only difference being the local potential $V(r)$ an electron feels at the interface which could depend on the sign of its spin, $E(V_{app})$ is the energy of an electron under an applied potential drop V_{app}, $g(E)$ are calculated from equations (6) and (7), $\hbar$ is the reduced Planck constant. The constant A is

$$A = \frac{16E}{V_0}\left(1 - \frac{E}{V_0}\right). \tag{22}$$

The prefactors concerning the subband LDOS stand for the effect of this term on transmission, i.e. if there is a great mismatch between the subband LDOS at the interfaces between the LHS and RHS FM electrodes for a given spin sign, there is reduced tunneling current with that spin polarization. We give the WKB formula above in its discrete form to be able to account for the 'arbitrariness' of the electrostatic potential across the barrier as this barrier can have significant variations as a function of polarization (even when homogeneous) and applied field, unavoidable necessitating a numerical treatment to calculate the currents in the spin channels. The spin-dependent potential barriers, $V_\uparrow(r)$ and $V_\downarrow(r)$ can be expressed in terms of the band parameters modified by the electrostatic and magnetochemical energies as:

$$V_{\uparrow,\downarrow}(r) = E_C^{FE} - E_F - \varnothing(r) \mp \mu_b H_m \tag{23}$$

where E_C^{FE} is the energy of the bottom of the conduction band of the FE layer, $\varnothing(r)$ is the local electrostatic potential at a coordinate r inside the FE layer, the $\mp\mu_b H_m$ term denotes the magnetochemical potential in the majority and minority spins near the Fermi level, E_f, in the FM electrode. Majority and minority spins have, in fact, separate E–k curves and form seperate 'conduction subband' curves as demonstrated via first principles calculations for FM materials [85] The amount of 'conduction subband' separation along easy axis such as [1 1 0] reported for Fe, Ni and Co vary from 2 eV to 0.6 eV [86] in very close proximity to the value we compute

J. Phys. D: Appl. Phys. **52** (2019) 015305

C Sen *et al*

in this paper (~0.85 eV) considering only the spin population near the Fermi level. A separation of subband energies directly mean that the majority and minority spins 'see' different barriers during tunneling. The FE TJ acts as an electrostatic barrier with the barrier height determined with respect to the energies of the majority and minority spins inside the conduction band of the FM metal under a given bias on the LHS electrode. In the calculations of the currents, $\varnothing(r)$ and H_m (see equation (8)) are found numerically from the solution of equation (1) that contains the terms in equations (5) and (9)–(11) assuming the condition that the polarization of the FE layer remains unchanged due to the great difference in the timescales of ferroelectric polarization dynamics and tunneling phenomena under pulsed bias. The charge distribution, ρ, however, will adapt rapidly to the applied bias and will be near-equilibrium as carrier relaxation times in a metallic medium is on the order of 10^{-14} seconds compared with bias durations of a few nanoseconds.

3. Results and discussion

3.1. FM/FE/FM with FE having homogeneous polarization

We first discuss the numerical results we obtained by imposing a homogeneous polarization to the FE layer in the FM/FE/ FM stack. The direction of the P_z is fixed at all times with dipoles pointing from the LHS electrode to the RHS to induce accumulation on the RHS electrode (tunnelling is therefore expected to occur from RHS FM to the LHS FM) as we always apply the positive bias to the LHS electrode (see figure 1). The opposite configuration (P_z pointing from RHS to LHS) will also yield exactly the same results owing to the symmetry of the stack and is not necessary to discuss. Equation (1) is solved along with the charge terms in equation (5) under fixed homogeneous P_z. FE polarization on its own would simply be expected to generate significant electric field penetration into the electrodes and therefore depolarizing fields inside the FE but our focus here is on the FM electrodes and the spin distribution.

The spin-dependent spatial carrier accumulation for various values of P_z both for zero and non-zero bias are provided in figure 3. Note in this plot that minority spin population away from the interfaces is not zero (red lines) but several orders of magnitude less than majority spin population. It is immediately visible in figure 3(c) that larger P_z values lead to minority spin accumulation at the interface in a FM electrode that contains otherwise majority spin electrons. This is a consequence of the electrostatic screening process and it is this very process that also leads to spin-mixing. With increasing bias, the region in which minority spins accumulate grows. For fixed P_z, the linear field dependent part of dielectric displacement, D_z, is the only bias sensitive part. This condition can be justified based on the approximation that most tunnelling experiments are measured under rapid pulsed voltages where P_z has no time to adapt to the rapidly changing voltage drops across the system. The carriers in a metallic medium, however, have relaxation times on the order of 10^{-12} seconds or less and will quickly establish their equilibrium distribution

satisfying equation (1) for pulsed bias durations of a few nanoseconds.

Spin mixing occurring at the FE/FM interfaces is strongly driven by the change in the subband DOS near the interfaces due to the need for electrostatic screening of the FE dipoles. The need arises because the electrostatic energy an electron would feel under the potential of unscreened polarization bound charges is several times more than the local magnetochemical potential. For electron energies limited to values around the Fermi energy, a strong local potential drop caused by the partially screened FE polarization charges could require carrier densities exceeding the subband states for the majority spins available in bulk. Looking at figure 4, for weak FE polarization in the TJ, we do not observe any change in the subband available states at the interfaces, which we call from here onwards local available states (LAS, given in density units of m^{-3}, see equations (6) and (7)) with respect to interior of the FM, hence a spin mixing will not be expected near the interface (see figure 3(a) for population density distribution). This is because the subband available states for the majority spins can accommodate sufficient local electron density (the population density) for the screening of FE polarization and the subband LAS for all spins remain almost unchanged at zero to moderate bias (<0.5 V). On the other hand, the subband LAS near the interfaces start to change for the case of moderate P_z amplitude (approx. 0.2 C m^{-2} here) and upon applying a low-to-mid positive bias to the LHS FM electrode, the region where the minority available states is comparable to majority ones extends slightly. Very importantly, the same conclusion was reached by first principles study in [87] wherein it was shown that the minority and majority subband LDOS near Fermi energy at the interface differ considerably from bulk for Fe 3d states, in the same manner, we show in this work, i.e. the minority spin subband available states increase at the interface compared to bulk values. The increase in the minority spin population near the Fermi level should be expected at the expense of an increase in the magnetochemical potential of carriers as further accumulation of majority spins for the screening of polarization charges would mean electrons populating higher energies and is not electrostatically favorable.

To provide a graphical guide to identify the possible regimes of FE polarization that allow spin polarized tunnelling and when spin polarization would disappear, we give the plot in figure 5. The averages of the majority and minority spin population density at the right FE/FM interface coordinate are provided along with the spin subband LAS near the Fermi level on the left FE/FM interface coordinate as a function of P_z at zero bias. In this plot, the population density is given in the positive axis and the subband LAS near the Fermi level on the LHS FM is in the negative axis for the convenience of comparison. Despite the obvious fact that precise numerical values here might differ for real experiments, it is clear that with increasing P_z, the spin polarization of the currents is expected to disappear as population densities of the majority and minority spins become identical in the RHS FM interface. In addition, note that, according to equation (23), the minority spins feel a 'higher potential' that causes an approx. 0.85 eV decrease in barrier for these carriers as well
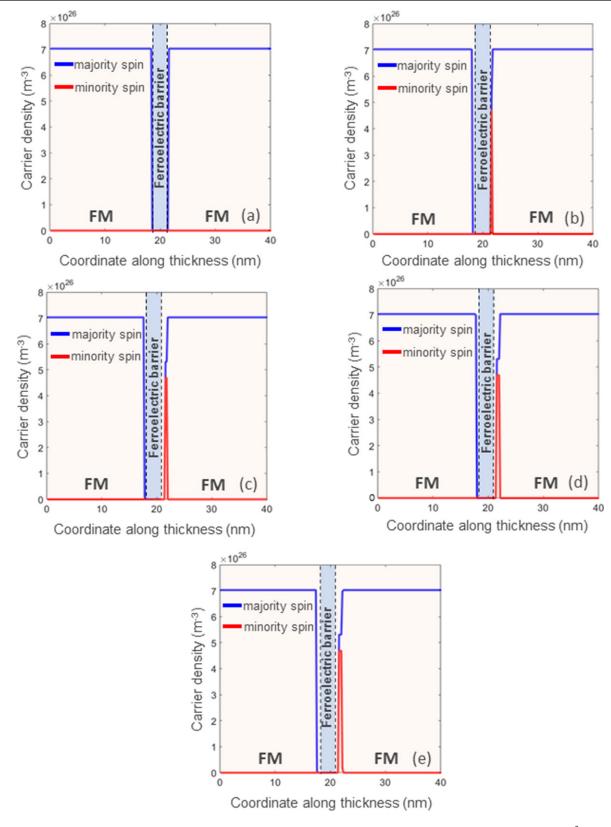
J. Phys. D: Appl. Phys. **52** (2019) 015305

C Sen *et al*

Figure 3. Average carrier population density at the RHS FE/FM interface induced by homogeneous P_z for (a) $P_z = 0.1$ C m^{-2}, (b) $P_z = 0.2$ C m^{-2} at 0 V bias, (c) $P_z = 0.2$ C m^{-2} at 0.5 V bias, (d) $P_z = 0.3$ C m^{-2} at 0 V bias and (e) $P_z = 0.3$ C m^{-2} at 0.5 V bias. Notice the minority spin acccumulation for increasing P_z as well as bias. For the case of $P_z = 0.1$ C m^{-2} no plot when under bias is given as there is no considerable change in minority spin population at the interface.
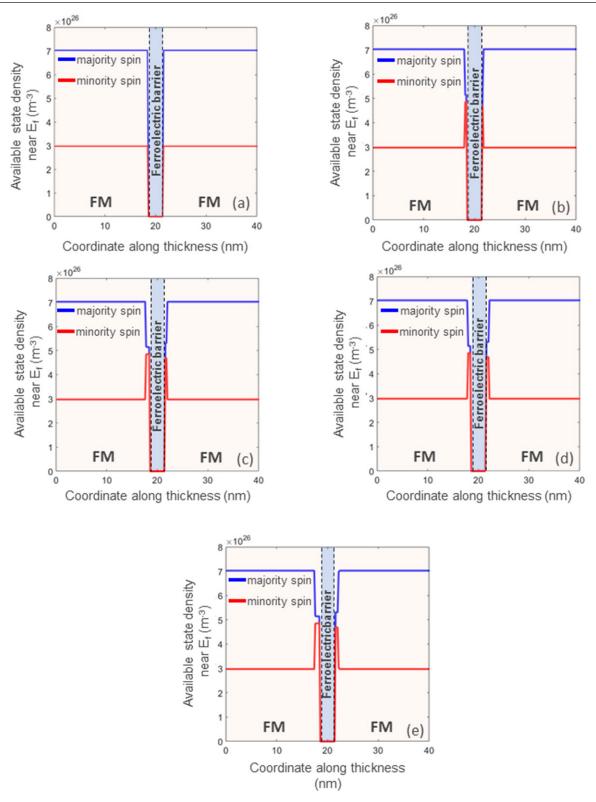
Figure 4. Average subband LDOS at the RHS FE/FM interface induced by homogeneous P_z for (a) $P_z = 0.1$ C m^{-2}, (b) $P_z = 0.2$ C m^{-2} at 0 V bias, (c) $P_z = 0.2$ C m^{-2} at 0.5 V bias, (d) $P_z = 0.3$ C m^{-2} at 0 V bias and (e) $P_z = 0.3$ C m^{-2} at 0.5 V bias. Notice the minority subband LDOS increasing at the interfaces for increasing P_z as well as bias.

(relative to the majority spins), allowing easier tunnelling for these carriers at any given bias, further diminishing the TMR. Voltage dependence of the spin polarization emanating from the different barriers the spins penetrate during tunnelling has been first explicitly analyzed in [35]. In addition to the

information given in that work, we argue that this difference in barrier heights tends to disappear for increasing P_z in the case of a FE TJ in the coming paragraphs.

As majority spins dominate the population density of the RHS FE/FM interface at low polarization (until around 0.15
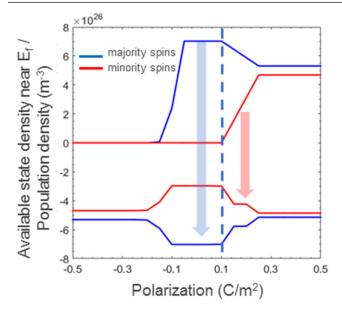
Figure 5. Average population density (positive vertical axis) at the RHS FE/FM interface and the subband LDOS (given in the negative vertical axis) at the LHS FM/FE interface as a function of P_z. The blue arrow denotes indicates that almost fully spin polarized tunnelling will occur from RHS FE/FM interface states to subband LDOS of the LHS FM/FE interface states. Beyond values of P_z around 0.15 C m^{-2} loss of spin polarization is expected as minority spin population starts to build up on the RHS FE/FM interface along with an increase in the minority subband LDOS on the LHS FM/FE interface as indicated by the shorter red arrow.

Figure 6. Total charge density across the trilayer indicating the exposed positive ionic sites on the LHS FM/FE interface and the carrier accumulation near the RHS FE/FM interface for 2 different P_z values. Stronger P_z causes a deeper penetration of the electric field to the RHS FM electrode increasing the effective barrier width to tunnelling for carriers on the LHS FE/FM interface.

C m^{-2}), there will be mostly majority spin tunneling below this regime to the available subband LAS at the RHS interface in the RHS FM electrode indicated by the thick blue arrow. The subband LAS near the Fermi level on the LHS electrode are at a maximum below 0.15 C m^{-2} (see figure 5). Once P_z is higher than this value, a gradual increase in minority spin population starts along with an increase in subband LAS of the minority and majority spins on the LHS electrode to which the tunnelling would be expected to occur, indicated by the red arrow. Strong amplitudes of P_z causes further spin mixing at the RHS and the subband LAS at the interface of the LHS electrode are almost identical, indicating that the tunnelling currents will not be spin polarized in this regime. In fact, moderate-to-strong applied bias (0.5–1 V) for when P_z is less than the critical value of 0.15 C m^{-2} here generates a similar effect: A bias of such magnitude can cause loss of spin polarization even if P_z is relatively weak analogous to the observations in dielectric TJs between FM electrodes. While bias can drive spin mixing at the interface causing a reduction in spin polarization, current amplitudes are expected to scale exponentially with applied bias. P_z determines both the spin polarization at the FM interfaces as well as the tunnel current amplitude in a symmetric FM/FE/FM stack. A strong P_z in the FE layer generates a 'deeper' penetration of the electric field into the LHS electrode, effectively increasing the barrier width. We give figure 6 to display the extent of field penetration that causes the exposure of positive charges on the LHS FM electrode and carrier accumulation on the RHS FM electrode interface. Electric field exposes the positive ions in the lattice on the RHS FM deeper into the electrode with
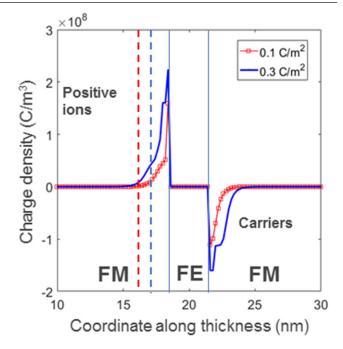
increasing P_z, thereby increasing effective barrier width. The left FM/FE interface undergoes carrier depletion as the negative pole of the FE polarization terminates at this interface thus repelling electrons away from the interface exposing the FM metal ions. Strong P_z values, apart from generating spin mixing, could thus cause a reduction in the tunnelling currents in the FE TJ for a given bias. This outcome is on top of the disappearance of the TMR effect in the tunnelling current amplitudes for majority and minority spin electrons as we discuss in the next paragraph.

The fundamental mechanism behind the spin mixing at the RHS FE/FM interface is therefore simply the 'need for electrostatic screening', which becomes dominant over the magnetic ordering of carriers in the FM. In other words, minimization of the electrostatic energy via screening of FE polarization charges via the carriers overwhelms the magnetochemical energy favoring magnetic order and could locally diminish magnetism on the RHS right FE/FM electrode interface. Considering, in addition, the spin sign dependence of the barrier, we calculated the average barrier heights for minority and majority spins as a function of P_z in the FE TJ from equation (23) and are displayed in figure 7. The different barrier heights for both spins follow a very gradual increase with increasing polarization in the TJ until around 0.15 C m^{-2}. This is the onset of minority spin accumulation that becomes energetically feasible near the interfaces, which then suddenly changes the electrostatic barrier for both majority and minority spins after which both carrier types experience similar barriers. A positive bias on the LHS FM electrode lowers the entire barrier regime as expected that drives the tunnelling currents. Both for zero and non-zero positive bias, the sudden
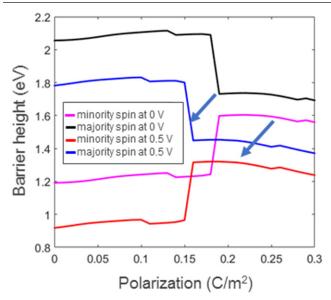
Figure 7. Average potential barrier height for minority (down) and majority (up) spins as a function of P_z for 0 V bias and 0.5 V bias. The potential barrier for both types of carriers is reduced by the application of bias as expected. The sudden change in the barrier heights corresponds to the regime when minority spin carriers participate in the screening of P_z.
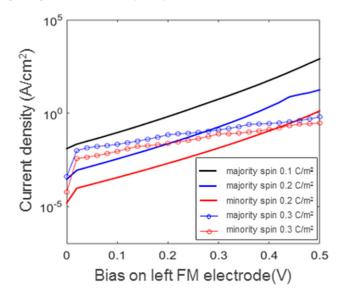

Figure 8. Tunnelling currents for minority and majority spins calculated using the WKB approximation for various homogeneous values of P_z (non-equilibrium, imposed P_z). As P_z gets stronger, mixed spin currents occur. For low P_z values (such as $P_z = 0.1$ C m^{-2} here) we find the current to be completely spin polarized and the down spin polarized currents are almost absent that cannot be plotted in the vertical log axis.

shift of the barriers occurring at a critical P_z value, however, is not accompanied by a sudden change in tunnelling currents (figure 8) obtained by the WKB method outlined in section 2.4. As explained in the previous paragraph, increasing the polarization value widens the effective physical barrier thickness due to the carrier depletion on the LHS FM/FE interface that counteracts the lowering of the electrostatic barrier, making the results of the WKB calculation vary smoothly with bias. It can immediately be noted from equations (20)

to (21) that an increase in the barrier thickness will dominate the currents as the exponent term in $T(E)$ depends on barrier thickness linearly while it depends on the square root of the potential barrier. Both channels of spin currents, therefore, diminish for stronger P_z as seen in figure 8. The relative difference in the magnetization orientation of the electrodes can generate a reduction in current magnitudes but such effects are due to the subband DOS altered by an externally applied magnetic field, which is the basis for the GMR effect.

3.2. FM/FE/FM with FE having polarization obtained from equation of state

The non-equilibrium homogeneous polarization case was analyzed to provide insight into the spin dependent screening process at the FM electrode interfaces. We now give the results for P_z obtained by solving equations (1), (15) and (16) as well as the charge distribution inside the FM electrodes at zero and finite bias. A multidomain state is highly feasible due to the finite penetration of the electric field into the FM electrodes. However, the asymmetric charge accumulation at the LHS FM/FE appears to be imposing a self-bias on the FE layer. Whether the formation of the single domain state is stable or metastable is a separate phenomenon and we take as reference the single domain state yielding results identical to experimental observations with FE TJs. When under bias, identical to the non-equilibrium homogeneous case, FE polarization is assumed to be fixed, non-responsive to the bias applied on the LHS electrode and only the linear term in equation (3) is changing in relation to equation (1). We first spontaneously solve the P_z along with the charge distributions inside the electrodes at zero bias and take this state as a reference for further calculations under bias. As expected, a size effect is observed where the value of P_z strongly depends on the thickness and the misfit introduced. Two different values of misfit are imposed on the FE layer as these allow us to compare the effect of two different P_z amplitudes and profiles. Although the in-plane component P_x was explicitly taken into account (see equations (15) and (16)), this component converged to zero implying a stable uniaxial FE for both misfit values. The misfit can vary in such structures depending on relaxation processes and defect content and the latter is kept outside the scope as they would seriously complicate the discussion. BaTiO$_3$ composition was used as a demonstrative case. We noted that the stability of sign of P_z is rather delicate due to the low thickness and the finite screening lengths of the electrodes. In fact, during the numerical solution of the potential, the direction of P_z and, therefore, the spin dependent carrier densities could alternate from left to right or vice versa. To remove this degeneracy condition separated by a low energy barrier in the double-well Landau potential, a small bias (0.01 V) was imposed to stabilize the polarization that makes it point from the LHS to the RHS electrode for which all discussions are carried out. We note that rather small polarization values are reported for FE TJs due to thickness effects [88–90], which appears to be in favor of spin polarized tunnelling in FM/FE/FM type stacks as discussed in section 3.1 due to relatively low electric fields expected at the interfaces. Identical trends in the
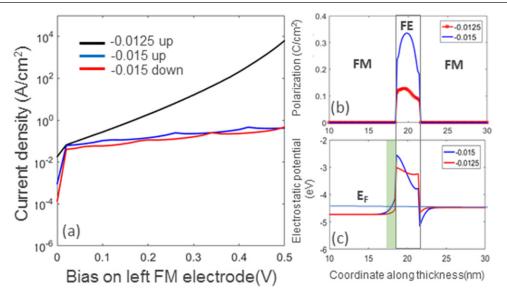
Figure 9. (a) Tunnelling currents for minority and majority spins calculated using the WKB approximation for values of P_z obtained from equations of state for 2 different misfit strains, (b) the P_z profiles across the thickness of the FE and (c) the profile of the barrier obtained by superimposing the solution of $\varnothing$ on the conduction band profiles of the stack.

spin distributions near the interfaces are obtained compared to the homogeneous polarization case with the difference that the near-equilibrium polarization has a curved profile (see figure 9). The inhomogeneous profile of P_z impacts the way dipoles terminate at the interfaces and has some influence on the interface carrier densities on the FM electrodes but does not change the physics discussed in the previous section.

Overall, the qualitative behavior of the FE TJ with equilibrium inhomogeneous polarization is the same as that of the homogeneous non-equilibrium polarization, making the discussion in the previous section applicable here, too. Small polarization values in the FE allow easier tunnelling and spin mixing at the interface from which tunnelling occurs is absent at small bias. For relatively weak polarization, the distance between the turning points which we take as a reference for barrier width to carry out the WKB calculations for the spin channels is also shorter as the field penetration into the LHS electrode is small. FE polarization determines the carrier accumulation/depletion at the interfaces and a bias (applied on the LHS FM electrode) does not change the qualitative picture. The large bias that exceeds the portions of the FE barrier profile in absolute value has been kept outside the scope of this work as the WKB calculations enter a different regime where $qV - E > 0$. Experimentally, however, one should expect the tunneling currents to follow the same trend as for the case $qV - E < 0$ considered here where the loss of the spin polarization is already demonstrated.

While the approach whose details are laid above captures the spin polarization behavior of tunneling currents in a general context, we would like to draw attention to the behavior of Co electrodes when interfacing a DE tunnel layer. In the case of Co, some groups have reported 'spin inversion' of the tunnelling currents, i.e. tunnelling currents mostly consist of minority spins [91]. This outcome was explained on the basis of local exchange interactions between Co and the constituents of the DE layer [92, 93]. Here, an antiparallel alignment

of the spins at the DE side of the interface can invert the subband LDOS of Co at the interface resulting in a local increase in minority spin population where the majority spin population can be surpassed. Thus, the screening is provided by these carriers and, as such, the spin polarized currents are expected to carry the minority spin sign.

4. Conclusions

In this work, we numerically studied the spin dependent screening process of FE polarization in FM/FE/FM TJs that are currently of interest for TMR-type devices and spintronics. Parallel magnetization of both FM electrodes was assumed. We demonstrated that the spin population at the interfaces is a strong function of the FE polarization and the applied bias on the system. The dependence of the TMR effect on FE polarization is an intrinsic response of the FM/FE/FM system and directly influences the states between which tunnelling occurs before considering any defect mediated spin flips and magnon-driven processes. With increasing values of FE polarization either due to the inherent composition of the FE or due to external bias, conservation of majority spin density at the interfaces becomes difficult, making spin-mixing inevitable. This occurs due to the need of the system to screen the FE polarization charges and reduce electrostatic energy. To fulfill this need, the majority and minority spin subband LAS near the Fermi level at the interfaces change to allow higher carrier population to be accommodated. This outcome is in excellent qualitative agreement with previous first principles results: The subband LDOS in Fe 3d band at the interface changes in favor of minority spins and decrease slightly for majority spins (with respect to bulk) when FE polarization points towards this interface. Our work thus provides an intuitive understanding of the dramatic effect of local electrostatic effects of the FE polarization on LDOS. Such a phenomenon naturally leads to the disappearance of the spin polarization of the tunnelling

J. Phys. D: Appl. Phys. **52** (2019) 015305

C Sen *et al*

currents. In addition, we calculated an abrupt change in barrier heights the spins feel under moderate bias (0.25–0.5 V) that is also expected to degrade spin polarization in currents. We note that a strong FE polarization component is not necessarily a positive parameter in FM/FE/FM junctions as a partial screening of the FE polarization effectively could increase the barrier height, resulting in smaller currents across the junction apart from the loss of spin polarization. Apart from the tunnelling barrier being spin dependent, the growth of the depletion zone inside the FM interfacing the negative pole of the FE dipoles is another reason that extends the effective barrier distance for tunneling. While it could very well be said that FE polarization allows magnetization control along the FM interface, whether a strong FE behavior is desired for TMR device design is questionable. As we write this, we keep in mind that a great variety of results have been reported in the literature for FE junctions in TMR studies but a general understanding of the trends in these systems is still lacking. Various FE compositions studied as TJs in TMR stacks are probably one cause of this lack of understanding: experimental results as a function of 'FE polarization strength' can vary greatly as we show here. In fact, we explicitly reveal here that any parameter inducing strong electric fields at the interfaces will lead to spin mixing at the interfaces, hence a reduction in TMR. We were also able to, therefore, demonstrate the connection between the spin dependent screening process at FE/FM interfaces and the variations of the TMR effect when under bias in such structures.

Acknowledgment

ORCID iDs

C Sen ● https://orcid.org/0000-0001-9416-6826
W A S Aldulaimi ● https://orcid.org/0000-0001-7709-9457
O Mohammadmoradi ● https://orcid.org/0000-0001-8126-4531
I B Misirlioglu ● https://orcid.org/0000-0002-6054-0119

References

[1] Sergienko I A and Dagotto E 2006 Role of the Dzyaloshinskii–Moriya interaction in multiferroic perovskites *Phys. Rev.* B **73** 094434

[2] Cheong S-W and Mostovoy M 2007 Multiferroics: a magnetic twist for ferroelectricity *Nat. Mater.* **6** 13–20

[3] Picozzi S *et al* 2008 Microscopic mechanisms for improper ferroelectricity in multiferroic perovskites: a theoretical review *J. Phys.: Condens. Matter* **20** 434208

[4] Ederer C and Fennie C J 2008 Electric-field switchable magnetization via the Dzyaloshinskii–Moriya interaction: FeTiO$_3$ versus BiFeO$_3$ *J. Phys.: Condens. Matter* **20** 434219

[5] Wang J *et al* 2003 Epitaxial BiFeO$_3$ multiferroic thin film heterostructures *Science* **299** 5

[6] Hill N A 2000 Why are there so few magnetic ferroelectrics? *J. Phys. Chem.* B **104** 6694–709

[7] Wolf S A *et al* 2001 Spintronics: a spin-based electronics vision for the future *Science* **294** 1488–95

[8] Fusil S *et al* 2014 Magnetoelectric devices for spintronics *Annu. Rev. Mater. Res.* **44** 91–116

[9] Ramesh R and Spaldin N A 2007 Multiferroics: progress and prospects in thin films *Nat. Mater.* **6** 21

[10] Chappert C, Fert A and Dau F 2007 The emergence of spin electronics in data storage *Nat. Mater.* **6** 813–23

[11] Nan C-W *et al* 2008 Multiferroic magnetoelectric composites: historical perspective, status, and future directions *J. Appl. Phys.* **103** 031101

[12] Žutić I, Fabian J and Sarma S D 2004 Spintronics: fundamentals and applications *Rev. Mod. Phys.* **76** 323

[13] Dagotto E 2002 *Nanoscale Phase Seperation and Colossal Magnetoresistance* (*Springer Series in Solid-State Sciences* vol XVIII) (Berlin: Springer) p 459

[14] Dagotto E, Hotta T and Moreo A 2001 Colossal magnetoresistant materials: the key role of phase separation *Phys. Rep.* **344** 153

[15] Ramirez A P 1997 Colossal magnetoresistance *J. Phys. Condens. Matter* **9** 8171–99

[16] Schmid H 1994 Multi-ferroic magnetoelectrics *Ferroelectrics* **162** 317–38

[17] Spaldin N A and Fiebig M 2005 The renaissance of magnetoelectric multiferroics *Science* **309** 391–2

[18] Khomskii D 2009 Classifying multiferroics: mechanisms and effects *Physics* **2** 20

[19] Eerenstein W, Mathur N D and Scott J F 2006 Multiferroic and magnetoelectric materials *Nature* **442** 759

[20] Wang K F, Liu J M and Ren Z F 2009 Multiferroicity: the coupling between magnetic and polarization orders *Adv. Phys.* **58** 321–448

[21] Alexandrov A S and Bratkovsky A M 1999 Theory of colossal magnetoresistance in doped manganites *J. Phys.: Condens. Matter* **11** 1989

[22] Cano A and Levanyuk A 2010 Pseudoproper ferroelectricity in thin films *Phys. Rev.* B **81** 172105

[23] Vaz C A F *et al* 2010 Temperature dependence of the magnetoelectric effect in Pb(Zr$_{0.2}$Ti$_{0.8}$)O$_3$/La$_{0.8}$Sr$_{0.2}$MnO$_3$ multiferroic heterostructures *Appl. Phys. Lett.* **97** 042506

[24] Vaz C A F *et al* 2011 Control of magnetism in Pb(Zr$_{0.2}$Ti$_{0.8}$)O$_3$/La$_{0.8}$Sr$_{0.2}$MnO$_3$ multiferroic heterostructures *J. Appl. Phys.* **109** 07D905

[25] Garcia V, Bibes M and Barthélémy A 2015 Artificial multiferroic heterostructures for an electric control of magnetic properties *C. R. Phys.* **16** 168–81

[26] Chu Y-H *et al* 2008 Electric-field control of local ferromagnetism using a magnetoelectric multiferroic *Nat. Mater.* **7** 478–82

[27] Thiele C *et al* 2007 Influence of strain on the magnetization and magnetoelectric effect in La$_{0.7}$A$_{0.3}$MnO$_3$/PMN-PT (0 0 1) (A = Sr,Ca) *Phys. Rev.* B **75** 054408

[28] Spurgeon S R *et al* 2014 Thickness-dependent crossover from charge- to strain-mediated magnetoelectric coupling in ferromagnetic/piezoelectric oxide heterostructures *ACS Nano* **8** 894–903

[29] Lou J *et al* 2009 Giant electric field tuning of magnetism in novel multiferroic FeGaB/lead zinc niobate–lead titanate (PZN-PT) heterostructures *Adv. Mater.* **21** 4711–5

[30] Bur A *et al* 2011 Giant electric-field-induced reversible and permanent magnetization reorientation on magnetoelectric Ni/(0 1 1) [Pb(Mg$_{1/3}$Nb$_{2/3}$)O$_3$]$_{(1−x)}$–[PbTiO$_3$]$_x$ heterostructure *Appl. Phys. Lett.* **98** 012504

J. Phys. D: Appl. Phys. **52** (2019) 015305

C Sen *et al*

[31] Jungho R *et al* 2001 Magnetoelectric properties in piezoelectric and magnetostrictive laminate composites *Japan. J. Appl. Phys.* **40** 4948

[32] Liu M *et al* 2009 Giant electric field tuning of magnetic properties in multiferroic ferrite/ferroelectric heterostructures *Adv. Funct. Mater.* **19** 1826–31

[33] Vaz C A F *et al* 2010 Magnetoelectric coupling effects in multiferroic complex oxide composite structures *Adv. Mater.* **22** 2900–18

[34] Zheng H *et al* 2004 Multiferroic BaTiO$_3$–CoFe$_2$O$_4$ nanostructures *Science* **303** 661–3

[35] Zhang S 1999 Spin-dependent surface screening in ferromagnets and magnetic tunnel junctions *Phys. Rev. Lett.* **83** 640–3

[36] Burton J D and Tsymbal E Y 2012 Magnetoelectric interfaces and spin transport *Phil. Trans. R. Soc.* A **370** 4840–55

[37] Bibes M, Villegas J E and Barthelemy A 2011 Ultrathin oxide films and interfaces for electronics and spintronics *Adv. Phys.* **60** 5–84

[38] Radaelli G *et al* 2014 Electric control of magnetism at the Fe/BaTiO$_3$ interface *Nat. Commun.* **5** 3404

[39] Spurgeon S R *et al* 2015 Polarization screening-induced magnetic phase gradients at complex oxide interfaces *Nat. Commun.* **6** 6735

[40] Meyer T L *et al* 2016 Enhancing interfacial magnetization with a ferroelectric *Phys. Rev.* B **94** 174432

[41] Lu H *et al* 2012 Electric modulation of magnetization at the BaTiO$_3$/La$_{0.67}$Sr$_{0.33}$MnO$_3$ interfaces *Appl. Phys. Lett.* **100** 232904

[42] Sharma M, Wang S X and Nickel J H 1999 Inversion of spin polarization and tunneling magnetoresistance in spin-dependent tunneling junctions *Phys. Rev. Lett.* **82** 616–9

[43] Moodera J S *et al* 1995 Large magnetoresistance at room temperature in ferromagnetic thin film tunnel junctions *Phys. Rev. Lett.* **74** 3273–6

[44] Miyazaki T and Tezuka N 1995 Giant magnetic tunneling effect in Fe/Al$_2$O$_3$/Fe junction *J. Magn. Magn. Mater.* **139** L231–4

[45] Miyazaki T, Yaoi T and Sio I 1991 Large magnetoresistance effect in ^{82}Ni-Fe/Al-Al$_2$O$_3$/Co magnetic tunneling junction *J. Magn. Magn. Mater.* **98** L7–9

[46] Gallagher W J *et al* 1997 Microstructured magnetic tunnel junctions *J. Appl. Phys.* **81** 3741–6

[47] Yuasa S *et al* 2004 Giant room-temperature magnetoresistance in single-crystal Fe/MgO/Fe magnetic tunnel junctions *Nat. Mater.* **3** 868

[48] Parkin S S P *et al* 2004 Giant tunnelling magnetoresistance at room temperature with MgO (1 0 0) tunnel barriers *Nat. Mater.* **3** 862

[49] Ikeda S *et al* 2010 A perpendicular-anisotropy CoFeB–MgO magnetic tunnel junction *Nat. Mater.* **9** 721

[50] Bowen M *et al* 2004 Large magnetoresistance in Fe/MgO/FeCo (0 0 1) epitaxial tunnel junctions on GaAs (0 0 1) *Appl. Phys. Lett.* **79** 1655–7

[51] Moodera J S, Nowak J and van de Veerdonk R J M 1998 Interface magnetism and spin wave scattering in ferromagnet-insulator-ferromagnet tunnel junctions *Phys. Rev. Lett.* **80** 2941–4

[52] Wen Z *et al* 2013 Ferroelectric-field-effect-enhanced electroresistance in metal/ferroelectric/semiconductor tunnel junctions *Nat. Mater.* **12** 617–21

[53] Maksymovych P *et al* 2009 Polarization control of electron tunneling into ferroelectric surfaces *Science* **324** 1421–5

[54] Yamada H *et al* 2013 Giant electroresistance of super-tetragonal BiFeO$_3$-based ferroelectric tunnel junctions *ACS Nano* **7** 5385–90

[55] Pantel D *et al* 2012 Tunnel electroresistance in junctions with ultrathin ferroelectric Pb(Zr$_{0.2}$Ti$_{0.8}$)O$_3$ barriers *Appl. Phys. Lett.* **100** 232902

[56] Boyn S *et al* 2014 High-performance ferroelectric memory based on fully patterned tunnel junctions *Appl. Phys. Lett.* **104** 052909

[57] Wang L *et al* 2016 Overcoming the fundamental barrier thickness limits of ferroelectric tunnel junctions through BaTiO$_3$/SrTiO$_3$ composite barriers *Nano Lett.* **16** 3911–8

[58] Bruno F Y 2016 Millionfold resistance change in ferroelectric tunnel junctions based on nickelate electrodes *Adv. Electron. Mater.* **2** 1500245

[59] Pantel D *et al* 2012 Reversible electrical switching of spin polarization in multiferroic tunnel junctions *Nat. Mater.* **11** 289

[60] Garcia V *et al* 2010 Ferroelectric control of spin polarization *Science* **327** 1106–10

[61] Zhuravlev M Y, Maekawa S and Tsymbal E Y 2010 Effect of spin-dependent screening on tunneling electroresistance and tunneling magnetoresistance in multiferroic tunnel junctions *Phys. Rev.* B **81** 104419

[62] Zhang S *et al* 1997 Quenching of magnetoresistance by hot electrons in magnetic tunnel junctions *Phys. Rev. Lett.* **79** 3744

[63] Davis A H and MacLaren J M 2000 Spin dependent tunneling at finite bias *J. Appl. Phys.* **87** 5224–6

[64] De Teresa J M *et al* 1999 Role of metal-oxide interface in determining the spin polarization of magnetic tunnel junctions *Science* **286** 507–9

[65] Bratkovsky A 1997 Spin tunneling in conducting oxides *MRS Fall Meeting (Boston)*

[66] Zhang J and White R M 1998 Voltage dependence of magnetoresistance in spin dependent tunneling junctions *J. Appl. Phys.* **83** 6512–4

[67] Valenzuela S O *et al* 2005 Spin polarized tunneling at finite bias *Phys. Rev. Lett.* **94** 196601

[68] Yin Y W *et al* 2011 Coexistence of tunneling magnetoresistance and electroresistance at room temperature in La$_{0.7}$Sr$_{0.3}$MnO$_3$/(Ba, Sr)TiO$_3$/La$_{0.7}$Sr$_{0.3}$MnO$_3$ multiferroic tunnel junctions *J. Appl. Phys.* **109** 07D915

[69] Quindeau A *et al* 2015 Four-state ferroelectric spin-valve *Sci. Rep.* **5** 9749

[70] Yin Y and Li Q 2017 A review on all-perovskite multiferroic tunnel junctions *J. Materiomics* **3** 245–54

[71] Hlinka J and Marton P 2006 Phenomenological model of a 90 degrees domain wall in BaTiO$_3$-type ferroelectrics *Phys. Rev.* B **74** 104104

[72] Tagantsev A K 2008 Landau expansion for ferroelectrics: which variable to use? *Ferroelectrics* **375** 19–27

[73] Butler W H *et al* 2001 Spin-dependent tunneling conductance of Fe|MgO|Fe sandwiches *Phys. Rev.* B **63** 054416

[74] Chikazumi S 1997 Physics of ferromagnetism *International Series of Monographs on Physics* vol 94, ed S F E J Birman *et al* (New York: Oxford University Press)

[75] Fert A and Campbell I A 1968 Two-current conduction in nickel *Phys. Rev. Lett.* **21** 1190–2

[76] Baibich M N *et al* 1988 Giant magnetoresistance of (0 0 1) Fe/(0 0 1)Cr magnetic superlattices *Phys. Rev. Lett.* **61** 2472

[77] Binasch G *et al* 1989 Enhanced magnetoresistance in layered magnetic structures with antiferromagnetic interlayer exchange *Phys. Rev.* B **39** 4828

[78] Stephanovich V A, Luk'yanchuk I A and Karkut M G 2005 Domain-enhanced interlayer coupling in ferroelectric/paraelectric superlattices *Phys. Rev. Lett.* **94** 047601

[79] Levanyuk A P and Misirlioglu I B 2011 Phase transitions in ferroelectric-paraelectric superlattices *J. Appl. Phys.* **110** 114109

[80] Misirlioglu I B, Kesim M T and Alpay S P 2014 Strong dependence of dielectric properties on electrical boundary

J. Phys. D: Appl. Phys. **52** (2019) 015305

C Sen *et al*

conditions and interfaces in ferroelectric superlattices *Appl. Phys. Lett.* **104** 022906

[81] Pertsev N A, Zembilgotov A G and Tagantsev A K 1998 Effect of mechanical boundary conditions on phase diagrams of epitaxial ferroelectric thin films *Phys. Rev. Lett.* **80** 1988–91

[82] Misirlioglu I B and Yildiz M 2014 Carrier accumulation near electrodes in ferroelectric films due to polarization boundary conditions *J. Appl. Phys.* **116** 024102

[83] Glinchuk M D, Eliseev E A and Stephanovich V A 2002 The depolarization field effect on the thin ferroelectric films properties *Physica* B **322** 356–70

[84] Jia C L *et al* 2007 Unit-cell scale mapping of ferroelectricity and tetragonality in epitaxial ultrathin ferroelectric films *Nat. Mater.* **6** 64–9

[85] Graz T 2016 Electron density of states for bcc iron http://lampx.tugraz.at/~hadley/ss1/materials/dos/iron.html (Accessed: 5 March 2018)

[86] Himpsel F J *et al* 1998 Magnetic nanostructures *Adv. Phys.* **47** 511–97

[87] Duan C-GJaswal S S and Tsymbal E Y 2006 Predicted magnetoelectric effect in Fe/BaTiO$_3$ multilayers: ferroelectric control of magnetism *Phys. Rev. Lett.* **97** 047201

[88] Junquera J and Ghosez P 2003 Critical thickness for ferroelectricity in perovskite ultrathin films *Nature* **422** 506

[89] Garcia V *et al* 2009 Giant tunnel electroresistance for non-destructive readout of ferroelectric states *Nature* **460** 81–4

[90] Petraru A *et al* 2008 Wedgelike ultrathin epitaxial BaTiO$_3$ films for studies of scaling effects in ferroelectrics *Appl. Phys. Lett.* **93** 072902

[91] LeClair P *et al* 2001 Sign reversal of spin polarization in Co/Ru/Al$_2$O$_3$/Co magnetic tunnel junctions *Phys. Rev.* B **64** 100406

[92] Lazić P, Belashchenko K D and Žutic I 2016 Effective gating and tunable magnetic proximity effects in two-dimensional heterostructures *Phys. Rev.* B **93** 241401

[93] Oleinik I I, Tsymbal E Y and Pettifor D G 2000 Structural and electronic properties of Co/Al$_2$O$_3$/Co magnetic tunnel junction from first principles *Phys. Rev.* B **62** 3952